Evolutionary comparisons reveal a positional switch for spindle pole oscillations in *Caenorhabditis* embryos

Soizic Riche,¹ Melissa Zouak,¹ Françoise Argoul,² Alain Arneodo,² Jacques Pecreaux,³ and Marie Delattre¹

¹Laboratory of Molecular Biology of the Cell, UMR5239, and ²Laboratory of Physics, UMR5672, Ecole Normale Supérieure de Lyon, Centre National de la Recherche Scientifique, 69007 Lyon, France

³Institute of Genetics and Developmental Biology, Centre National de la Recherche Scientifique, UMR6290, University of Rennes 1, 35043 Rennes, France

uring the first embryonic division in Caenorhabditis elegans, the mitotic spindle is pulled toward the posterior pole of the cell and undergoes vigorous transverse oscillations. We identified variations in spindle trajectories by analyzing the outwardly similar one-cell stage embryo of its close relative Caenorhabditis briggsae. Compared with C. elegans, C. briggsae embryos exhibit an anterior shifting of nuclei in prophase and reduced anaphase spindle oscillations. By combining physical perturbations and mutant analysis in both species, we show

that differences can be explained by interspecies changes in the regulation of the cortical $G\alpha$ –GPR–LIN-5 complex. However, we found that in both species (1) a conserved positional switch controls the onset of spindle oscillations, (2) GPR posterior localization may set this positional switch, and (3) the maximum amplitude of spindle oscillations is determined by the time spent in the oscillating phase. By investigating microevolution of a subcellular process, we identify new mechanisms that are instrumental to decipher spindle positioning.

Introduction

O

0

JOURNAL

The first embryonic asymmetric division of the nematode *Caenorhabditis elegans* has been essential to reveal the biophysical and molecular mechanisms controlling nuclei and spindle positioning (Gönczy, 2008). In *C. elegans* and in many other nematode species, the mitotic spindle is asymmetrically localized at the end of the first cell cycle, giving rise to a small posterior cell and a large anterior cell after cytokinesis (Brauchle et al., 2009). In a preliminary study, we found that spindle trajectories inside the cell differed between species and from those observed in the reference species *C. elegans*. In this work, we used the differences found in one of *C. elegans* closest known relatives, *Caenorhabditis briggsae*, as variant phenotypes to further explore the mechanisms of nuclei and spindle positioning.

In *C. elegans*, pronuclei meet at the posterior end of the cell after fertilization. During prophase, unbalanced pulling forces act on the astral microtubules, leading to the centration and rotation of the assembled nuclei–centrosome complex (NCC) along the anterior/posterior (A/P) axis of the cell

M. Zouak and F. Argoul contributed equally to this paper.

Correspondence to Marie Delattre: marie.delattre@ens-lyon.fr

Abbreviations used in this paper: A/P, anterior/posterior; DIC, differential interference contrast; NCC, nuclei–centrosome complex; NEBD, nuclear envelope breakdown.

(Labbé et al., 2004; Kimura and Onami, 2005). At the onset of mitosis, cortical-force generators pull on the astral microtubules with stronger forces toward the posterior pole (Grill et al., 2001; Labbé et al., 2004; McCarthy Campbell et al., 2009). During anaphase, therefore, the spindle is posteriorly displaced and undergoes transverse oscillations, whose amplitude reflects the strength of these pulling forces (Pecreaux et al., 2006; Redemann et al., 2011).

Proteins involved in cortical pulling forces form a complex that is functionally conserved from worms to mammals to control spindle positioning (Werts et al., 2011). In *C. elegans*, this complex contains the G protein Gα subunit, which is anchored to the cortex. Gα binds the G protein regulators GPR-1 and GPR-2 (referred to as GPR-1/2), which bind the NuMA homologue, LIN-5. LIN-5 interacts with the minus end–directed motor dynein. The anchoring of dynein to the cortex via this ternary complex, in conjunction with depolymerizing astral microtubules, is thought to generate pulling forces (Gönczy, 2008). GPR-1/2 and LIN-5 are found at the cortex and show a

© 2013 Riche et al. This article is distributed under the terms of an Attribution–Noncommercial–Share Alike–No Mirror Sites license for the first six months after the publication date (see http://www.rupress.org/terms). After six months it is available under a Creative Commons License (Attribution–Noncommercial–Share Alike 3.0 Unported license, as described at http://creativecommons.org/licenses/by-nc-sa/3.0/).

Supplemental Material can be found at: http://jcb.rupress.org/content/suppl/2013/05/16/jcb.201210110.DC1.html

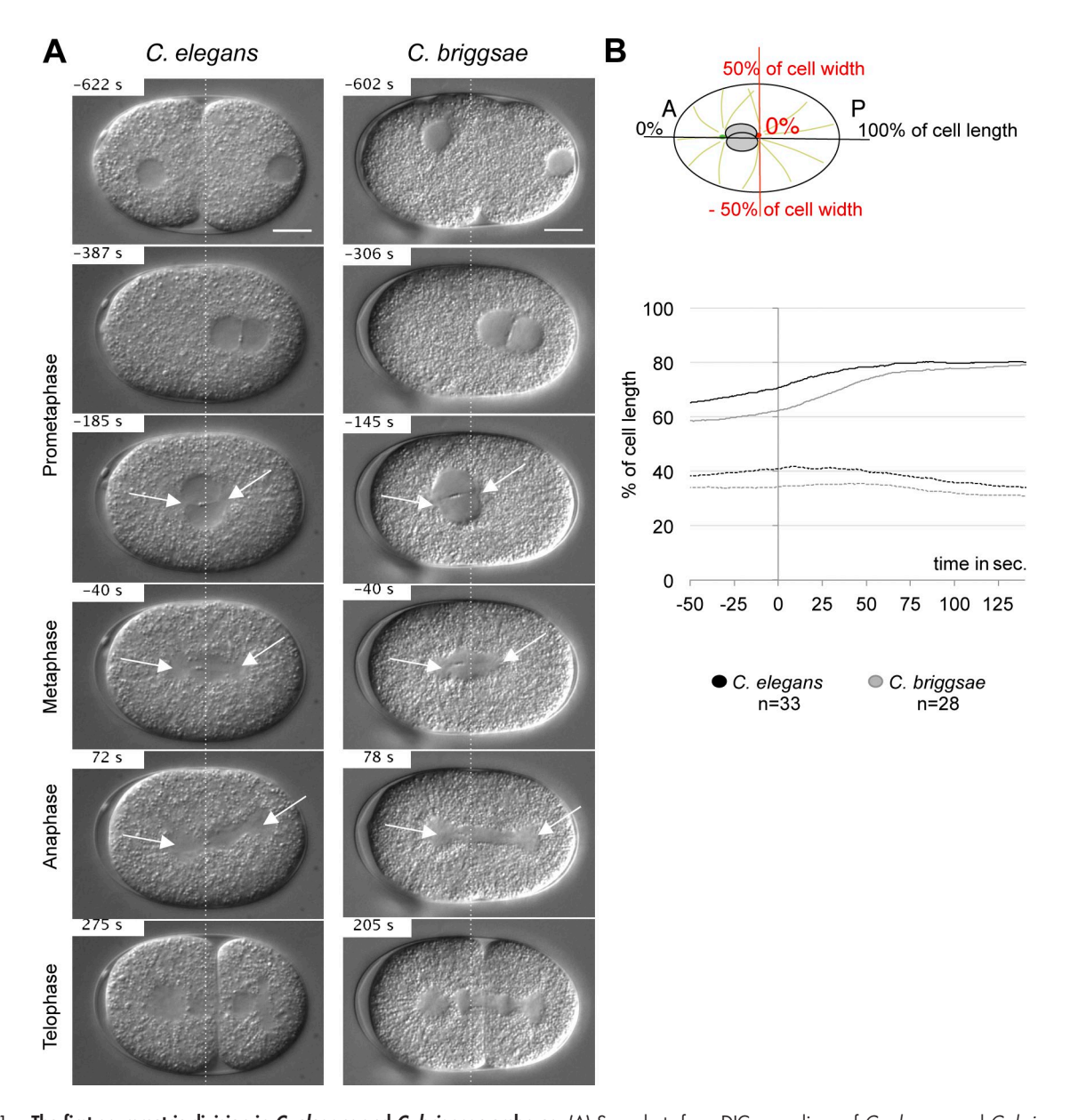


Figure 1. **The first asymmetric division in** *C. elegans* **and** *C. briggsae* **embryos.** (A) Snapshots from DIC recordings of *C. elegans* and *C. briggsae* wild-type strains. Time is shown relative to anaphase onset (t = 0 s). Anterior is to the left. Broken lines are positioned at 50% of embryo length. Arrows show the asters. Bars, 10 µm. (B) Drawing of a one-cell stage embryo. The horizontal axis corresponds to the A/P axis: 0% defines the anterior pole of the cell. The transverse axis is in red: 0% is the center of the cell. On the bottom panel, the mean position of the centrosome along the A/P axis is shown relative to anaphase onset (t = 0 s) for both species. –50 s corresponds to metaphase and 125 s to cytokinesis onset. Solid and broken lines represent the posterior and anterior centrosomes, respectively.

slight enrichment at the anterior cortex during NCC centration/ rotation and at the posterior cortex during mitosis (Colombo et al., 2003; Gotta et al., 2003; Park and Rose, 2008). Thus, the dynamic localization of GPR-1/2/LIN-5 correlates with the direction of forces throughout the cell cycle and may reflect the position of active force generators. However, inactivation of G α or GPR-1/2 slows down but does not prevent NCC centration in *C. elegans* (Goulding et al., 2007; Park and Rose, 2008), which suggests that mechanisms independent of the ternary complex act in parallel to position the NCC in the cell center. Such mechanisms involve cortical dynein-dependent gliding of microtubules or cytoplasmic dynein pulling along microtubule length (Gusnowski and Srayko, 2011; Kimura and Kimura, 2011).

We found two main differences in spindle trajectories between *C. elegans* and *C. briggsae* embryos that may reflect differential regulation of intracellular forces. We explored these phenotypes using a combination of physical perturbation of the mitotic spindle and analysis of mutant or RNAi phenotypes in both species.

Results and discussion

NCC and spindle positioning differ between C. elegans and C. briggsae embryos

To analyze nuclei and spindle movements of both *C. elegans* N2 and *C. briggsae* JU1018 strains, we tracked the position of both

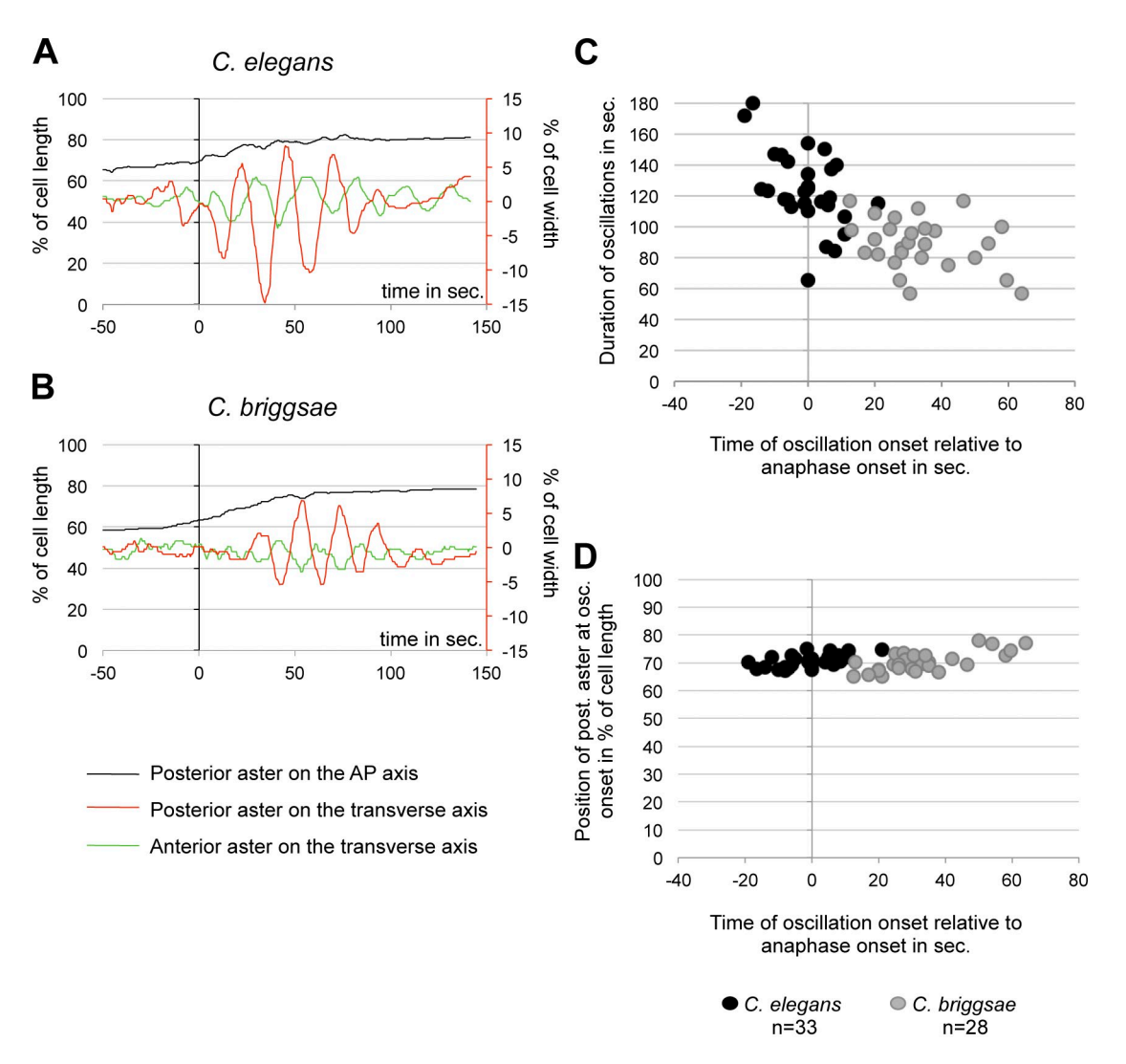


Figure 2. **Spindle oscillations differ between** *C. elegans* and *C. briggsae* embryos. (A and B) Centrosome displacement on the A/P (y axis on the left) and transverse axes (y axis on the right) relative to anaphase onset (t = 0 s) for one representative embryo per species. The position of the posterior centrosome on the A/P axis is represented by a black curve, while its position on the transverse axis is shown in red. Transverse movements of the anterior centrosome are shown in green. (C) The onset and end of posterior centrosome oscillations were measured manually from graphs of transverse oscillations (see A and B). Oscillation duration for each embryo is represented relative to the time at oscillation onset (in seconds from anaphase onset). (D) The position of the posterior centrosome in percentage of cell length at the beginning of oscillation is plotted versus the time at oscillation (in seconds from anaphase onset).

asters over time from differential interference contrast (DIC) recordings. Although the NCC formed at the posterior side of the cell in both species, it was systematically displaced beyond the center of the cell in *C. briggsae* embryos. Because of this "overcentration," the metaphase spindle formed more anteriorly in *C. briggsae* than in *C. elegans*. At the end of anaphase, however, the posterior spindle pole reached the same final position in both species (as a percentage of total cell length; Fig. 1, A and B; Videos 1 and 2; and Table S1).

Another important difference between these species involved the spindle oscillations during anaphase. Although the frequency of oscillations was similar between species, we found a strong diminution in oscillation amplitude for both centrosomes in *C. briggsae* embryos compared with *C. elegans* (Fig. 2, A and B; and Table S1). Moreover, the spindle began to oscillate at anaphase onset in *C. elegans* embryos, whereas it started 30 s later in *C. briggsae* embryos. As oscillations ended at the same time

in both species, they lasted 30 s less in C. briggsae than those in C. elegans (Fig. 2 C and Table S1). We also found a correlation between oscillation onset and a specific position of the posterior centrosome along the A/P axis, corresponding to $\sim 70\%$ of embryo length in both species and in C. elegans embryos with genetically altered size (Fig. 2 D, Fig. S1 A, and Table S1).

We then repeated the same measurements using two other *C. elegans* and *C. briggsae* strains. We confirmed that the observed spindle trajectories were not strain-specific but rather reflected a consistent interspecies divergence (Table S1).

Because *C. briggsae* is more frequently found in tropical regions and can grow at higher temperatures than *C. elegans* (Dolgin et al., 2008), we grew and recorded *C. briggsae* animals at 28°C. These embryos still exhibited different spindle trajectories compared with *C. elegans* embryos raised at 23°C (Table S1). For these cellular processes, therefore, differences between species do not result from thermal adaptations of *C. briggsae* animals.

The position of the posterior centrosome dictates oscillation onset in both species

We first investigated the conserved correlation between oscillation onset and position of the posterior centrosome along the A/P axis. We tested the existence of a positional control for oscillation onset. Because the posterior centrosome was located at 62.9% at anaphase onset in *C. briggsae* embryos, the oscillation delay found in this species could result from the time it took the posterior centrosome to reach 70% (in *C. elegans* the posterior centrosome was already located at 70.9% at anaphase onset; Table S1). Alternatively, the time delay observed in oscillation onset could reflect a delay in the activation of cortical force generators between species.

To determine whether spindle oscillations are temporally or spatially controlled, we forced the mitotic spindle of C. briggsae embryos to reach 70% of cell length earlier in the cell cycle. To this end, anterior astral microtubules were severed using a laser microbeam at the end of prometaphase (Fig. 3, A and B; and Video 3). For experiments performed around nuclear envelope breakdown (NEBD), microtubule severing had only a mild effect on spindle displacement. Cuts performed after NEBD, however, successfully displaced the mitotic spindle toward the posterior end of the cell. Thus, unbalanced microtubule pulling forces are initiated after NEBD, as previously described for C. elegans embryos (Labbé et al., 2004; McCarthy Campbell et al., 2009). After microtubule severing, oscillations began when the posterior centrosome reached $68.9 \pm 1.8\%$ of the embryo's length, regardless of the elapsed time (Fig. 3 C). Oscillation onset, therefore, depends on the position of the posterior centrosome. In addition, oscillations within laser-cut C. briggsae embryos lasted longer and exhibited larger amplitudes than wild-type embryos (Fig. 3, D and E). We conclude that: (1) force-generator activity is temporally regulated, (2) a positional switch controls the onset of spindle oscillations, (3) delayed spindle oscillations observed in C. briggsae are a consequence of the overcentration phenotype, and (4) the lower amplitude oscillations that characterize intact C. briggsae embryos are in part caused by the shorter time spent in the oscillating phase. Precise coordination of oscillation onset and the start of anaphase in C. elegans prevented the identification of this positional switch.

GPR posterior localization correlates

with the positional switch in both species

In *C. elegans*, the enrichment of GPR/LIN-5 at the posterior cortex corresponds to \sim 70% of cell length during anaphase (Fig. 4, A and J; Park and Rose, 2008), which suggests that these proteins may set the positional switch for oscillation onset. We asked if *C. briggsae* embryos showed the same pattern of GPR localization.

First, we confirmed that the $G\alpha$ –GPR–LIN-5 complex is functionally conserved in *C. briggsae* embryos. After inactivation of each member of this complex, we found reduced spindle elongation, no spindle displacement, and no spindle oscillations during anaphase, while embryonic polarity was not affected (Fig. S1, B–E; Fig. S2 A; and Video 4). We also showed that the cortical localization of *C. briggsae* GPR-2 (Cbr-GPR-2)

depends on $G\alpha$ proteins, as shown for *C. elegans* embryos (Fig. S2, B–D). Last, we performed laser microsurgery of the central spindle during anaphase (Grill et al., 2001) and revealed unbalanced pulling forces acting on astral microtubules (Fig. S1 F). Thus, in *C. briggsae* embryos, $G\alpha$ –GPR–LIN-5–dependent asymmetric pulling forces are also involved in spindle positioning and oscillations during anaphase.

Next, we found that Cbr-GPR-2 localization shows dynamic patterns during the first cell cycles (Fig. S2 B). In anaphase embryos, similar to *C. elegans* embryos, levels of cortical Cbr-GPR-2 were low in the cell center while a steep increase was detected around 70% of embryo length (Fig. 4, B and J). In both species, therefore, the enrichment of posterior cortical GPR coincides with the positional switch for oscillation onset.

GPR localization influences the oscillation onset; GPR levels act on oscillation amplitude

In *C. elegans*, GPR acts on anaphase spindle oscillations in a dose-dependent manner (Pecreaux et al., 2006; Redemann et al., 2011). Interestingly, the *C. briggsae* genome contains one *gpr* gene, whereas *C. elegans* has two, which is consistent with having reduced spindle oscillations in *C. briggsae*. We first tested whether the difference in gene copy number is responsible for the different spindle motion observed between species.

We first analyzed *C. briggsae* embryos from the ANA017 line expressing an excess of Cbr-GFP-GPR-2. Although these embryos still exhibited NCC overcentration, anaphase spindle oscillations were closer to *C. elegans* oscillations in amplitude. Reciprocally, *C. elegans* mutants for either *gpr-1* or *gpr-2* displayed smaller transverse oscillations that were similar to *C. briggsae* oscillations in amplitude (Fig. 4 I, Fig. 5 A, and Videos 5 and 6). However, modification of *gpr* gene copy number in both species had no impact on the onset of spindle oscillations, both in position and time (Fig. 4, G and H). Moreover, we did not observe changes in the domain boundary of GPR in these conditions, reinforcing the correlation between GPR localization and oscillation onset. (Fig. 4, C, D, and J). Thus, interspecies changes in GPR levels may only explain the differences observed in the amplitude of oscillations.

To test a direct role of GPR on oscillation onset, we attempted to affect the size of the GPR domain. Although we could not identify experimental conditions leading to a change in position of the GPR transition zone, we analyzed embryos for which GPR decorates the entire cortex. We reasoned that if GPR is present above the centrosomes when cortical motors are turned on, microtubules could be prematurely captured. Consequently, oscillations would be triggered when the spindle is in a more central position. In C. briggsae embryos, as in C. elegans, we found that GPR invades the entire cortex after removal of the $G\beta$ subunit of heterotrimeric G proteins (Thyagarajan et al., 2011) or the DEP domain protein LET-99 (Tsou et al., 2003; Fig. 4, E and F). Importantly, the onset of spindle oscillations was precocious in time and position in both conditions. We also found increased oscillation amplitude compared with wild-type C. briggsae, which is consistent with our previous observation

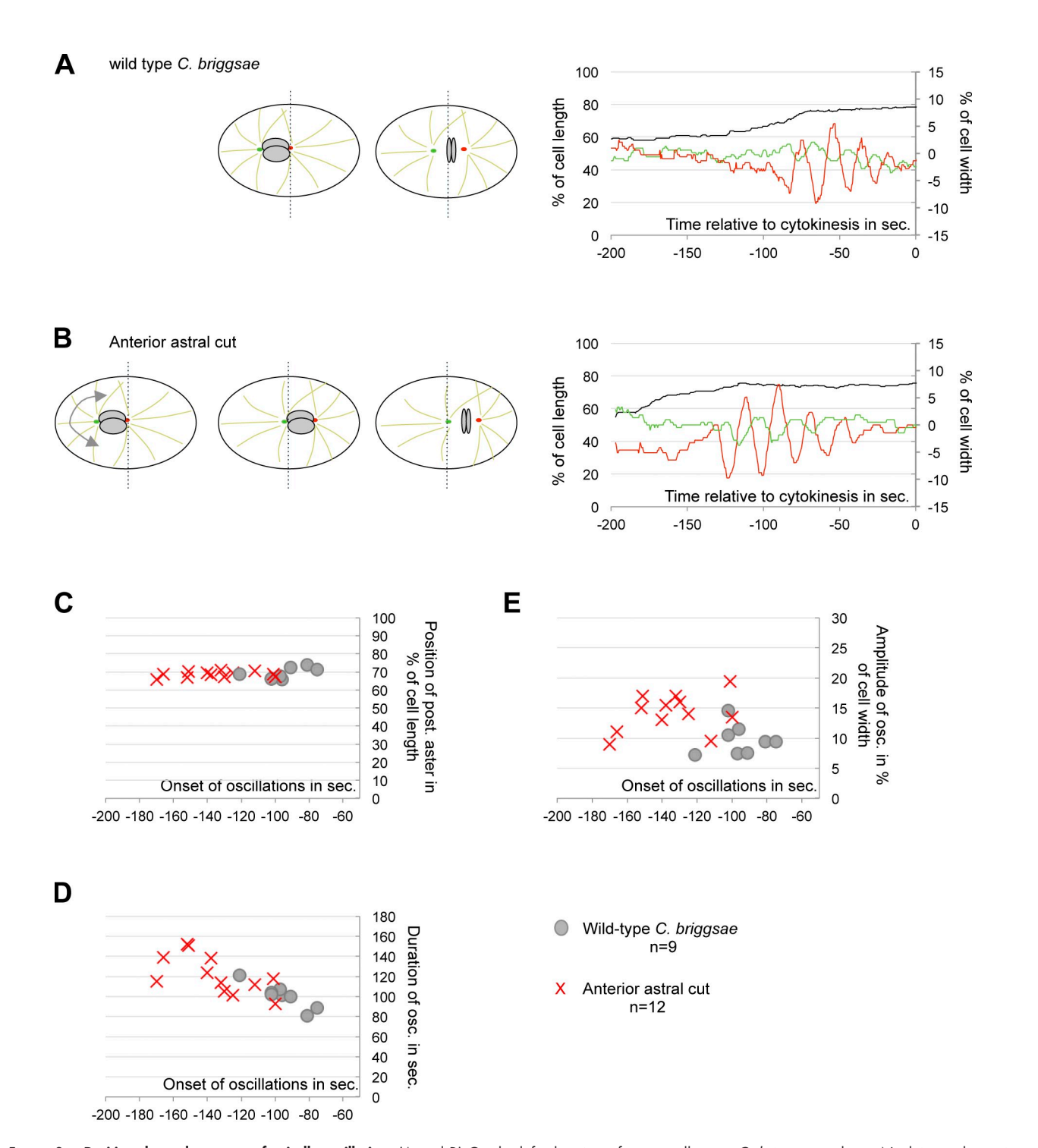


Figure 3. **Position-dependent onset of spindle oscillation.** (A and B) On the left, drawing of a one-cell stage *C. briggsae* embryo. Nuclei are shown in gray, microtubules in light green, the anterior centrosome in green, and the posterior centrosome in red. The broken line represents the cell center. On the right, the position of the posterior centrosome along the A/P axis (black curve) and the transverse movements of both centrosomes (green and red curves) are shown relative to cytokinesis onset (t = 0 s). One representative embryo is shown, among the 9 intact embryos (A) and 12 embryos in which the anterior astral microtubules have been severed (B) that were analyzed. (C–E) From cut and intact embryos, measures of the position of the posterior centrosome at oscillation onset (C), oscillation duration in seconds (D), and maximum amplitude of posterior centrosome oscillations (E) are shown relative to the time at oscillation onset (in seconds to cytokinesis onset).

that earlier oscillation onset allows larger oscillation amplitudes (Fig. 4, G–I; and Videos 7 and 8).

We expected higher oscillation amplitude in Cbr- $G\beta(RNAi)$ embryos compared with Cbr-let-99(RNAi), because Cbr- $G\beta(RNAi)$ embryos combine high levels of cortical GPR and premature

oscillations onset (Fig. 4, E and F). We found, however, a similar amount of total GPR protein in wild-type and Cbr- $G\beta(RNAi)$ embryos (Fig. S2 F), which suggests that despite its cortical accumulation, GPR is still a limiting factor to sustain strong oscillations in Cbr- $G\beta(RNAi)$ embryos. To test this hypothesis,

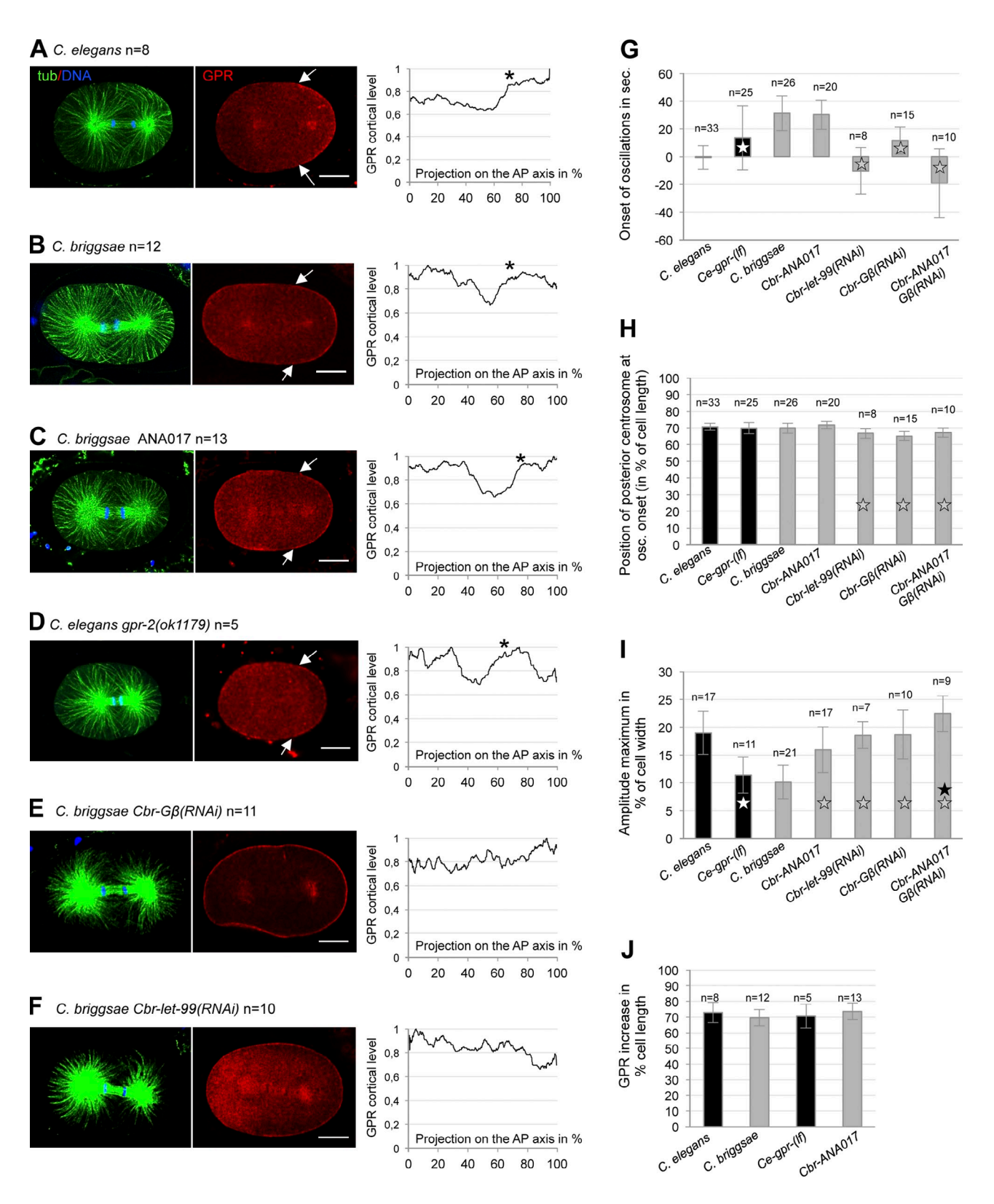


Figure 4. GPR sets the spatial switch for oscillations. (A-F) Plots represent the mean cortical intensity of GPR (from 0 to 1) from n anaphase embryos stained with GPR (red), tubulin (green), and DNA (blue) and normalized to the maximum intensity. Values have been projected onto the A/P axis, from the anterior pole (0%) to the posterior pole (100%). The asterisks represent the edge of the posterior plateau. One representative embryo is shown on the left. Anterior is to the left. Arrows show the edge of the GPR posterior domain. Bars, 10 µm. (G-I) Histograms from analysis of oscillation curves. Ce-gpr-(If) corresponds to gpr-1(ok2126) or gpr-2(ok1179) mutant embryos. Statistical differences are shown with white, gray, or black stars for comparison to wild-type C. elegans, wild-type C. briggsae, or Cbr-Gβ(RNAi), respectively (for P < 0.05). Error bars represent standard deviation. The time at posterior centrosome oscillation onset relative to anaphase onset is shown in G, the position of the posterior centrosome at oscillation onset is shown in H, and the maximum amplitude of oscillations is shown in I. (J) Position of the edge of the GPR plateau on the A/P axis was measured from individual graphs of GPR cortical intensities in A-D. Mean values are shown, error bars indicate standard deviation.

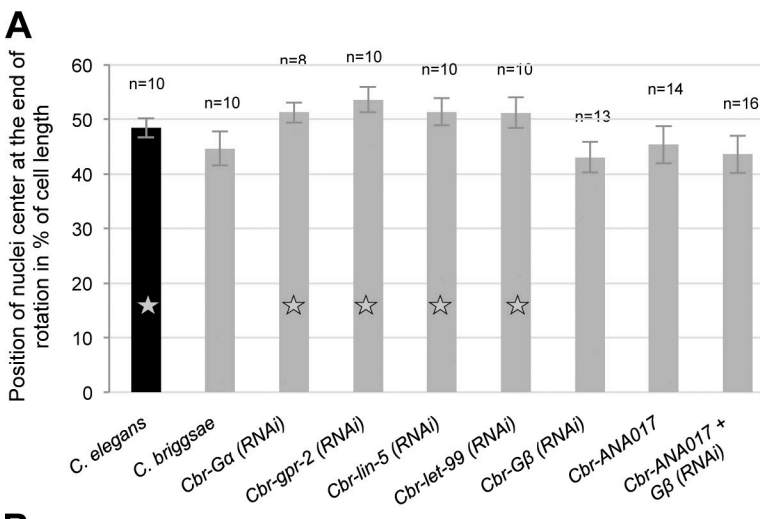
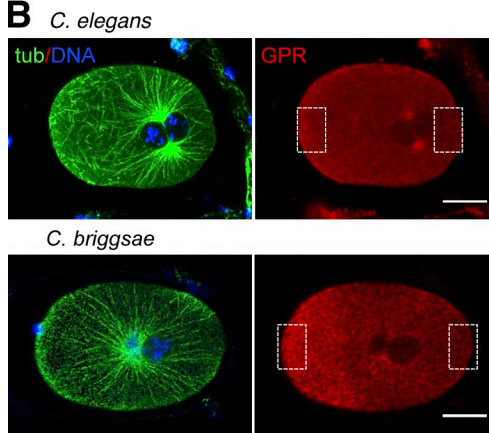
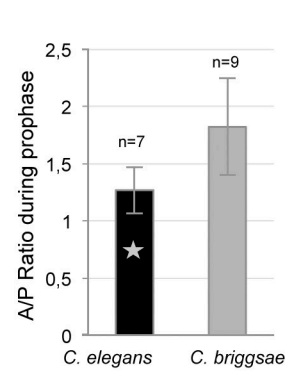


Figure 5. An up-regulation of G α -GPR-LIN-5 leads to NCC overcentration in *C. briggsae* embryos. (A) Position of the center of the NCC at the end of its rotation is represented as a percentage of cell length. Error bars indicate standard deviation. Statistical differences are shown with a star for comparison to wild-type *C. briggsae* (for P < 0.05). (B) *C. elegans* and *C. briggsae* embryos during NCC rotation stained with antibodies against GPR (in red). Tubulin is in green and DNA in blue. Rectangles show the region where GPR intensity was measured. The anterior pole is to the left. Bar, 10 µm. The histogram shows the mean ratio of GPR levels between anterior and posterior side of the cell for each species. Error bars indicate standard deviation. The star shows statistical difference between species (P < 0.05).





we treated the ANA017 line showing an excess of GPR with Cbr- $G\beta(RNAi)$. We found a further increase in oscillation amplitude compared with single Cbr- $G\beta(RNAi)$ or ANA017 embryos (Fig. 4, G–I). Thus, the increased oscillations found in Cbr- $G\beta(RNAi)$ embryos are not caused by an excess of GPR but rather by premature oscillations and expanded GPR domain, as found in Cbr-let-99(RNAi) embryos. We confirm, therefore, that the amplitude of oscillations is dependent on the time spent in the oscillating phase as well as the level of available GPR. Overall, we show that the posterior aster starts to oscillate prematurely when GPR is found all over the cortex, which is consistent with a role of GPR in setting the positional switch.

$G\alpha$ -GPR-LIN-5-dependent forces are responsible for NCC overcentration in *C. briggsae* embryos

We finally explored the mechanisms leading to NCC overcentration in *C. briggsae* embryos. In *C. elegans*, down-regulation of GPR or LIN-5 during prophase is needed to prevent NCC overcentration (Galli et al., 2011; Panbianco et al., 2008). We found that inactivation of $G\alpha$, GPR, or LIN-5 by RNAi abolished nuclei overcentration in *C. briggsae* embryos (Fig. 5 A and Fig. S1 B), which suggests that a constitutive up-regulation of the $G\alpha$ –GPR–LIN-5 complex is responsible for NCC overcentration in this species. Importantly, down-regulation of all three proteins restored nuclei centering in *C. briggsae*, which

suggests that mechanisms independent on the ternary complex might, however, be conserved between species to control nuclei centering (Gusnowski and Srayko, 2011; Kimura and Kimura, 2011). Because the different forces responsible for nuclei positioning can be phenotypically uncoupled in *C. briggsae* embryos, their analysis in this satellite species should lead to important findings.

Interestingly, we noticed a strong enrichment of Cbr-GPR-2 in the anterior side of *C. briggsae* embryos during prophase, which persisted throughout the first cell cycle (Figs. 4 B, 5 B, and S2 A). We quantified the A/P ratio of GPR in both species during prophase and found a higher asymmetry toward the anterior pole for *C. briggsae* embryos compared with *C. elegans* (Fig. 5 B). Although this observation is only a positive correlation, we propose that *C. briggsae* embryos are characterized by a lack of $G\alpha$ -GPR-LIN-5 inhibition during prophase, which leads to an accumulation of GPR at the anterior side of the cell and to NCC overcentration.

Despite the anterior accumulation of Cbr-GPR-2, the anterior centrosome undergoes very little oscillation during anaphase and remains almost static in *C. briggsae* embryos (Figs. 1 B and 2 B). We postulated that this anterior GPR pool does not contribute to strong pulling forces during anaphase. To address this question, we inactivated Cbr-PAR-2 protein in *C. briggsae* embryos. In *C. elegans*, *par-2* mutant embryos show an "anteriorization" of the cortex leading to symmetric and weak GPR

cortical recruitment and consequently reduced anaphase pulling forces (Grill et al., 2001). In Cbr-par-2(RNAi) embryos, we found symmetric cell division, reduced spindle elongation, and an absence of oscillations, which strongly suggests a reduction of cortical pulling forces (Fig. S1, B-E). However, we found a uniform and strong signal of Cbr-GPR-2 in Cbr-par-2(RNAi) embryos at all stages (Fig. S2 D). These results suggest that the anterior pool of Cbr-GPR-2 has a different activity between prophase and anaphase in C. briggsae embryos. Cbr-GPR-2 and Ce-GPR-1/2 proteins display only 76% of sequence similarity. Therefore, changes in the protein sequence itself might be responsible for the differences in localization and activation found between species. Identifying these evolutionary changes will be of great interest to decipher the mechanisms of GPR regulation.

Cryptic changes in spindle trajectories behind a conserved positional switch

Our comparative analysis allowed us to uncover a conserved positional switch for spindle oscillation onset. We propose that in both C. elegans and C. briggsae embryos, the GPR posterior localization sets this positional switch, while the level of GPR within the posterior domain controls the amplitude of transverse oscillations. We also revealed two main evolutionary changes: (1) a differential regulation of GPR during prophase leading to NCC overcentration and consequently to shorter time in the oscillation phase for C. briggsae embryos, and (2) a different availability of GPR during anaphase. The diminished transverse oscillations that characterize C. briggsae embryos result from a combination of these two differences. With this study, we show that the first cell division of nematode embryos is associated with cryptic changes that can serve to explore essential cellular functions.

How does the positional switch function? It has been previously proposed that spindle oscillations are caused by a gradual increase in processivity of force generators over time (Pecreaux et al., 2006). Our results suggest that although force generators are activated, they are engaged only when the aster is close enough to the domain of force generators, which contain GPR. We reasoned that when asters are far from the GPR domain, few microtubules are long enough to be captured by motors at a given time point. This would lead to aster displacement but be insufficient to trigger oscillations. As the aster gets closer to that domain, enough microtubules may reach the cortex before switching to catastrophe and more motors become progressively engaged.

Although spindle oscillations are instrumental to unravel the mechanisms of microtubule-based forces, they have no inherent function. Why are mechanisms controlling spindle oscillation onset maintained across nematode evolution? A sudden increase in pulling forces may help to rapidly propel the posterior centrosome (and the entire spindle) toward a most posterior position or alternatively to oppose a breaking transversal force to posterior spindle displacement. In any cases, the positional switch could ensure final spindle position and thus asymmetric cell division regardless of initial spindle position and remaining time to cytokinesis.

Materials and methods

The Bristol N2 C. elegans strain was used as the standard wild type. The JU1018 strain, an RNAi-sensitive derivative of the wild-type Indian AF16 strain, was used as the reference for C. briggsae (Nuez and Félix, 2012). We found that AF16 and JU1018 have undistinguishable phenotypes concerning the two first embryonic divisions. The following additional strains were used: C. elegans VC1670 gpr-1(ok2126), C. elegans RB1150 gpr-2 (ok 1 179) (two loss-of-function alleles, referred to as Ce-gpr-(If); Caenorhabditis Genetics Center), and C. briggsae RW20000 Cbr-unc-119(st20000) (Zhao et al., 2010). We analyzed other wild isolates of both species that were both geographically and genetically distinct from the reference strains: C. elegans CB4856 and LKC34, and C. briggsae ED3092 and HK104. C. briggsae and C. elegans strains were handled similarly on nematode growth medium (NGM) plates, cultured at 20°C and fed on OP50 bacteria. Fluorescent lines and Cbr-unc-119 worms were maintained at 25°C. Embryos were recorded at 23°C unless stated otherwise.

Transgenic C. briggsae strains

We amplified the full-length Cbr-gpr-2, Cbr-par-2, and Cbr-par-6 from AF16 genomic DNA. The genes were then cloned at the C terminus of GFP in the TH303 plasmid (a gift from T. Hyman, Max Planck Institute, Dresden, Germany), under the control of the C. elegans pie-1 promoter and 3' UTR. The vector also contains the C. elegans unc-119 gene and promoter. These plasmids were used at 4 µg/µl for coating on gold beads, and beads were then placed on macrocarriers in a hepta-adapter of a Biolistic PDS-1000 HE system (Bio-Rad Laboratories). Cbr-unc-119 worms (Zhao et al., 2010) were plated and bombarded two times at 1,500 psi. We obtained five independent integrated lines for Cbr-GPR-2, one for Cbr-PAR-6, and one for Cbr-PAR-2. All lines were then backcrossed to the JU1018 strain to obtain worms sensitive to RNAi by ingestion. All lines displayed wild-type phenotypes except one Cbr-GFP::GPR-2 line that exhibited the strongest cortical GFP signal. Embryos from this line ANA017 displayed rocking of the NCC during overcentration and stronger spindle oscillations.

Gene inactivation by RNAi

RNAi experiments were performed by ingestion of transformed HT115 bacteria in both species. Cbr-gpb-1 (Gβ), Cbr-gpr-2, Cbr-lin-5, Cbr-goa-1, Cbr-gpa-16, Cbr-par-2, and Cbr-let-99 genes were amplified from AF16 genomic DNA and cloned into the L4440 plasmid. 48-64 h of feeding at 20°C was needed to obtain the strongest phenotypes in C. briggsae JU1018 embryos. Cbr-G α (RNAi) corresponds to a double inactivation of Cbr-gpa-16 and Cbr-goa-1 genes. After inactivation of let-99 or $G\beta$ by RNAi in C. elegans, the uninterrupted rocking of NCC and spindle prevented us from determining the onset of mitotic oscillations. However, NCC and mitotic spindle oscillations were clearly distinguishable after RNAi treatment of these genes in C. briggsae embryos, allowing us to measure anaphase oscillation onset. cid-1 and C27D9.1 genes were reported to affect embryo size in C. elegans embryos (from http://www.worm .mpi-cbg.de/phenobank/cgi-bin/MenuPage.py). After inactivation of cid-1, we obtained minute embryos, whereas inactivation of C27D9.1 gave very long embryos. In both cases, embryos were viable and showed no other visible phenotypes.

Recording, tracking, and statistics

Embryos were mounted in M9 onto a 2% agarose pad between a slide and a coverslip and observed on a microscope (Axio Imager A2; Carl Zeiss) equipped with a 100× Plan-Apochromat NA 1.4 lens. We took two images per second from pronuclear appearance to the second cell division using a digital camera (DX4-285FW; Kappa) and the corresponding timelapse module. We defined t = 0 s as the separation of chromosomes at anaphase onset, which is detectable on DIC recordings. All embryos were recorded at 23°C. We found that cell cycle duration was similar between species at this temperature (Table S1). To track nuclei and centrosome position over time, we used the "Manual Tracking" plugin from ImageJ (National Institutes of Health). During mitosis, cortical contractions are reduced and embryo length is constant. This allowed us to set the anterior side of the cell as the spatial reference point. Positions were expressed in percentage of embryo length, with 0% representing the anterior pole and 100% representing the posterior pole. Graphs of centrosome position on the A/P axis and transverse axis as a function of time were analyzed with MATLAB software (MathWorks). In a first stage, low-frequency trends of the transverse centrosome displacements were corrected by a third-order fitting with a polynomial. In a second stage, a low-pass filter was applied to correct the signal for high-frequency noise. The intersections of the oscillation signal (beyond a predefined time) with the horizontal axis (corresponding to zero transverse displacement) were first detected by a dichotomic algorithm, and then the local extrema for each oscillation were detected in between the successive pairs of intersection points. From these extrema positions, we computed amplitudes and the period of each half-oscillation. The onset and end of oscillations were detected manually from those graphs.

For all measurements, statistical significance was measured using a two-tailed Student's t test.

Astral microtubule severing experiments

Embryos were visualized by DiC using a laser microdissection microscope (LMD; Leica) equipped with a pulsed N2 laser ($\lambda=337$ nm). After completion of nuclei/centrosome rotation, a curve was drawn around the centrosome to cut astral microtubules (as depicted in Fig. 4 A). Because astral microtubules grow extremely quickly (Srayko et al., 2005), we expected that the microtubule network and spindle behavior would be restored a few seconds after the cut. For these experiments, the onset of cytokinesis, assessed by the onset of furrowing, was taken as the reference time point because we could not detect anaphase onset on the laser-equipped microscope. To make sure that heat from the laser did not perturb the embryos, we measured the time from NEBD to the onset of cytokinesis. In wild-type embryos, this interval was 203.4 \pm 31.7 s, which was not statistically different from the cut embryos (217.9 \pm 34.8 s, P = 0.37).

Antibody production and stainings

Cbr-GPR-2 shares only 76% similarity with the nearly identical Cel-GPR-1/2 proteins. This prevented us from detecting Cbr-GPR-2 using antibodies directed against C. elegans GPR-1/2 (gifts from P. Gönczy, École Polytechnique Fédérale de Lausanne, Lausanne, Switzerland; and L. Rose, University of California, Davis, Davis, CA; Colombo et al., 2003; Park and Rose, 2008). We raised a polyclonal antibody against two conserved peptides of GPR-1/2 and Cbr-GPR-2. Eurogentec performed peptide production and rabbit immunization. One rabbit serum yielded a strong GPR signal on fixed C. briggsae embryos (1:50) but not on C. elegans fixed embryos, nor on a Western blot. Gravid hermaphrodites were placed on polylysine-coated slides and cut open. A coverslip was then placed on the released embryos and excess liquid was removed to flatten the eggs. Slides were placed on frozen aluminum blocks. Once frozen, the coverslip was cracked and slides were plunged in -20°C methanol for at least 5 min. Slides were then rinsed in PBS and stained at room temperature for 45 min for each primary and secondary antibody. The following primary antibodies were used: rabbit anti-Cel-GPR-1 (1:50; Park and Rose, 2008), rabbit anti-GFP (1:500; A6455; Invitrogen), and mouse anti-tubulin (1:100; DM1a; Sigma-Aldrich). Secondary antibodies were a donkey Dylight488 anti-mouse (Jackson ImmunoResearch Laboratories, Inc.), and a donkey Cy3 anti-rabbit (1:2,000; Jackson ImmunoResearch Laboratories, Inc.). DNA was revealed with Hoechst 33342 (Sigma-Aldrich). Stained embryos were imaged using a spectral confocal microscope (SP5; Leica) or a spectral confocal microscope (LSM710; Zeiss), and images were processed with ImageJ. Single confocal planes are shown on the figures.

Quantification of GPR levels

For staining on C. briggsae embryos, we used either the anti-Cbr-GPR-2 antibody on wild-type embryos, or anti-GFP antibodies on transgenic lines expressing GFP::Cbr-GPR-2. Except in Fig. 4 D, we used a Cbr-GFP::GPR-2 line displaying wild-type phenotypes to assess GPR levels. C. briggsae embryos stained with the antibody against Cbr-GPR-2 are shown on Fig. S2 A. GFP signals from the Cbr-GFP-GPR-2 transgenic line are shown on Fig. 4 (B, C, E, and F), Fig. 5 B, and Fig. S2 (B–D). GPR quantification was performed from mid-plane single confocal images. Only late metaphase and anaphase one-cell embryos were processed for Fig. 4, as the GPR domain is expanding in telophase embryos. First, a 5-pixel line was drawn on the embryo cortex using ImageJ, and pixel intensity was measured using the "Plot profile" function. Using MATLAB, we detected the embryo contour from these images and computed its barycentric coordinates, and the symmetric long axis and the transverse axis of the embryo were plotted. This reference frame was used to convert the two-dimensional coordinates of the GPR contour data into cell-length percentages. For each embryo, the half top or bottom cortices were treated separately, as they often displayed different profiles. The number of embryos processed is shown on Fig. 4, corresponding to several cortices varying between n and 2n. To measure the A/P ratio of GPR levels in prophase embryos, we quantified pixel intensity in a large cytoplasmic region in both species, as depicted in Fig. 5 B.

Western blots

Cbr-GFP::GPR-2 lines were synchronized and L3 larvae were then fed for 48 h on NGM plates seeded with bacteria expressing $Cbr\text{-}G\beta$ double-stranded RNA (dsRNA), a control RNAi (*C. elegans unc-22*), or control NGM plates. From these worms, embryonic extracts were prepared and loaded onto SDS-PAGE gels. A mouse anti-tubulin antibody (DM1a; Sigma-Aldrich) was used at 1:2,000 as a loading control. A mouse monoclonal anti-GFP antibody (Roche) was used at 1:1,000 as a readout of GPR overall levels. Primary antibodies were stained overnight at 4°C. Anti-mouse secondary antibodies were used at 1:5,000 (NA931; GE) for 40 min at room temperature.

Online supplemental material

Fig. S1 shows that $G\alpha$ -GPR-LIN-5-dependent unbalanced pulling forces control the first cell division of C. briggsae embryos. Fig. S2 shows Cbr-GPR-2 localization and levels in C. briggsae wild-type and RNAi-treated embryos. Video 1 shows a time-lapse DIC recording of a wild-type C. elegans N2 embryo. Video 2 shows a time-lapse DIC recording of a wild-type briggsae JU1018 embryo. Video 3 shows a time-lapse DIC recording of a wild-type C. briggsae JU1018 embryo after laser severing of anterior astral microtubules using a pulsed N2 laser from a Leica LMD microscope (λ = 337 nm). Video 4 shows a time-lapse DIC recording of a C. briggsae embryo treated with Cbr-gpr-2(RNAi). Video 5 shows a time-lapse DIC recording of a C. briggsae embryo from the ANA017 line, in which Cbr-GPR-2 is found in excess. Video 6 shows a time-lapse DIC recording of a C. briggsae embryo treated with Cbr-GB (RNAi). Video 7 shows a time-lapse DIC recording of a C. briggsae embryo treated with Cbr-let-99(RNAi). Table S1 shows quantification of events in C. elegans and C. briggsae strains. Online supplemental material is available at http://www.jcb.org/ cgi/content/full/jcb.201210110/DC1.

This work has been initiated in the laboratory of M.-A. Félix. We are very grateful to her for help and fruitful discussions. We thank P. Gönczy, M.-A. Félix, and anonymous reviewers for critical reading of the manuscript. We thank A. Khalil and D. Cluet for help with image processing, N. Bozonnet for technical help, and the Plateau Technique Imagerie/Microscopie (PLATIM) imaging facility of the Unité Mixte de Service Biosciences (Lyon, France). We thank the Gönczy laboratory for sharing its laser-equipped microscope. Some nematode strains used in this work were provided by the Caenorhabditis Genetics Center, which is funded by the National Institutes of Health National Center for Research Resources (NCRR).

This project has been funded by grants from the Centre National de la Recherche Scientifique (ATIP) and the ARC foundation to M. Delattre. S. Riche is supported by a PhD fellowship from the Region Rhône-Alpes.

Submitted: 22 October 2012 Accepted: 11 April 2013

References

- Brauchle, M., K. Kiontke, P. MacMenamin, D.H. Fitch, and F. Piano. 2009. Evolution of early embryogenesis in rhabditid nematodes. *Dev. Biol.* 335: 253–262. http://dx.doi.org/10.1016/j.ydbio.2009.07.033
- Colombo, K., S.W. Grill, R.J. Kimple, F.S. Willard, D.P. Siderovski, and P. Gönczy. 2003. Translation of polarity cues into asymmetric spindle positioning in *Caenorhabditis elegans* embryos. *Science*. 300:1957–1961. http://dx.doi.org/10.1126/science.1084146
- Dolgin, E.S., M.A. Félix, and A.D. Cutter. 2008. Hakuna Nematoda: genetic and phenotypic diversity in African isolates of *Caenorhabditis elegans* and *C. briggsae*. *Heredity* (*Edinb*). 100:304–315. http://dx.doi.org/10.1038/sj .hdy.6801079
- Galli, M., J. Muñoz, V. Portegijs, M. Boxem, S.W. Grill, A.J. Heck, and S. van den Heuvel. 2011. aPKC phosphorylates NuMA-related LIN-5 to position the mitotic spindle during asymmetric division. *Nat. Cell Biol.* 13: 1132–1138. http://dx.doi.org/10.1038/ncb2315
- Gönczy, P. 2008. Mechanisms of asymmetric cell division: flies and worms pave the way. *Nat. Rev. Mol. Cell Biol.* 9:355–366. http://dx.doi.org/10 .1038/nrm2388
- Gotta, M., Y. Dong, Y.K. Peterson, S.M. Lanier, and J. Ahringer. 2003. Asymmetrically distributed *C. elegans* homologs of AGS3/PINS control spindle position in the early embryo. *Curr. Biol.* 13:1029–1037. http:// dx.doi.org/10.1016/S0960-9822(03)00371-3
- Goulding, M.B., J.C. Canman, E.N. Senning, A.H. Marcus, and B. Bowerman. 2007. Control of nuclear centration in the *C. elegans* zygote by receptorindependent Gα signaling and myosin II. *J. Cell Biol.* 178:1177–1191. http://dx.doi.org/10.1083/jcb.200703159

- Grill, S.W., P. Gönczy, E.H. Stelzer, and A.A. Hyman. 2001. Polarity controls forces governing asymmetric spindle positioning in the *Caenorhabditis elegans* embryo. *Nature*. 409:630–633. http://dx.doi.org/10.1038/35054572
- Gusnowski, E.M., and M. Srayko. 2011. Visualization of dynein-dependent microtubule gliding at the cell cortex: implications for spindle positioning. *J. Cell Biol.* 194:377–386. http://dx.doi.org/10.1083/jcb.201103128
- Kimura, K., and A. Kimura. 2011. A novel mechanism of microtubule length-dependent force to pull centrosomes toward the cell center. *Bioarchitecture*. 1:74–79. http://dx.doi.org/10.4161/bioa.1.2.15549
- Kimura, A., and S. Onami. 2005. Computer simulations and image processing reveal length-dependent pulling force as the primary mechanism for *C. elegans* male pronuclear migration. *Dev. Cell.* 8:765–775. http://dx.doi.org/10.1016/j.devcel.2005.03.007
- Labbé, J.C., E.K. McCarthy, and B. Goldstein. 2004. The forces that position a mitotic spindle asymmetrically are tethered until after the time of spindle assembly. J. Cell Biol. 167:245–256. http://dx.doi.org/10.1083/jcb.200406008
- McCarthy Campbell, E.K., A.D. Werts, and B. Goldstein. 2009. A cell cycle timer for asymmetric spindle positioning. *PLoS Biol.* 7:e1000088. http:// dx.doi.org/10.1371/journal.pbio.1000088
- Nuez, I., and M.A. Félix. 2012. Evolution of susceptibility to ingested doublestranded RNAs in *Caenorhabditis* nematodes. *PLoS ONE*. 7:e29811. http://dx.doi.org/10.1371/journal.pone.0029811
- Panbianco, C., D. Weinkove, E. Zanin, D. Jones, N. Divecha, M. Gotta, and J. Ahringer. 2008. A casein kinase 1 and PAR proteins regulate asymmetry of a PIP(2) synthesis enzyme for asymmetric spindle positioning. *Dev. Cell.* 15:198–208. http://dx.doi.org/10.1016/j.devcel.2008.06.002
- Park, D.H., and L.S. Rose. 2008. Dynamic localization of LIN-5 and GPR-1/2 to cortical force generation domains during spindle positioning. *Dev. Biol.* 315:42–54. http://dx.doi.org/10.1016/j.ydbio.2007.11.037
- Pecreaux, J., J.C. Röper, K. Kruse, F. Jülicher, A.A. Hyman, S.W. Grill, and J. Howard. 2006. Spindle oscillations during asymmetric cell division require a threshold number of active cortical force generators. *Curr. Biol.* 16:2111–2122. http://dx.doi.org/10.1016/j.cub.2006.09.030
- Redemann, S., S. Schloissnig, S. Ernst, A. Pozniakowsky, S. Ayloo, A.A. Hyman, and H. Bringmann. 2011. Codon adaptation-based control of protein expression in *C. elegans. Nat. Methods*. 8:250–252. http://dx.doi .org/10.1038/nmeth.1565
- Srayko, M., A. Kaya, J. Stamford, and A.A. Hyman. 2005. Identification and characterization of factors required for microtubule growth and nucleation in the early *C. elegans* embryo. *Dev. Cell.* 9:223–236. http://dx.doi .org/10.1016/j.devcel.2005.07.003
- Thyagarajan, K., K. Afshar, and P. Gönczy. 2011. Polarity mediates asymmetric trafficking of the Gbeta heterotrimeric G-protein subunit GPB-1 in C. elegans embryos. Development. 138:2773–2782. http://dx.doi.org/10.1242/dev.063354
- Tsou, M.F., A. Hayashi, and L.S. Rose. 2003. LET-99 opposes Galpha/GPR signaling to generate asymmetry for spindle positioning in response to PAR and MES-1/SRC-1 signaling. *Development*. 130:5717–5730. http://dx.doi.org/10.1242/dev.00790
- Werts, A.D., M. Roh-Johnson, and B. Goldstein. 2011. Dynamic localization of C. elegans TPR-GoLoco proteins mediates mitotic spindle orientation by extrinsic signaling. Development. 138:4411–4422. http://dx.doi.org/10 .1242/dev.070979
- Zhao, Z., S. Flibotte, J.I. Murray, D. Blick, T.J. Boyle, B. Gupta, D.G. Moerman, and R.H. Waterston. 2010. New tools for investigating the comparative biology of *Caenorhabditis briggsae* and *C. elegans. Genetics*. 184:853–863. http://dx.doi.org/10.1534/genetics.109.110270

Riche et al., http://www.jcb.org/cgi/content/full/jcb.201210110/DC1

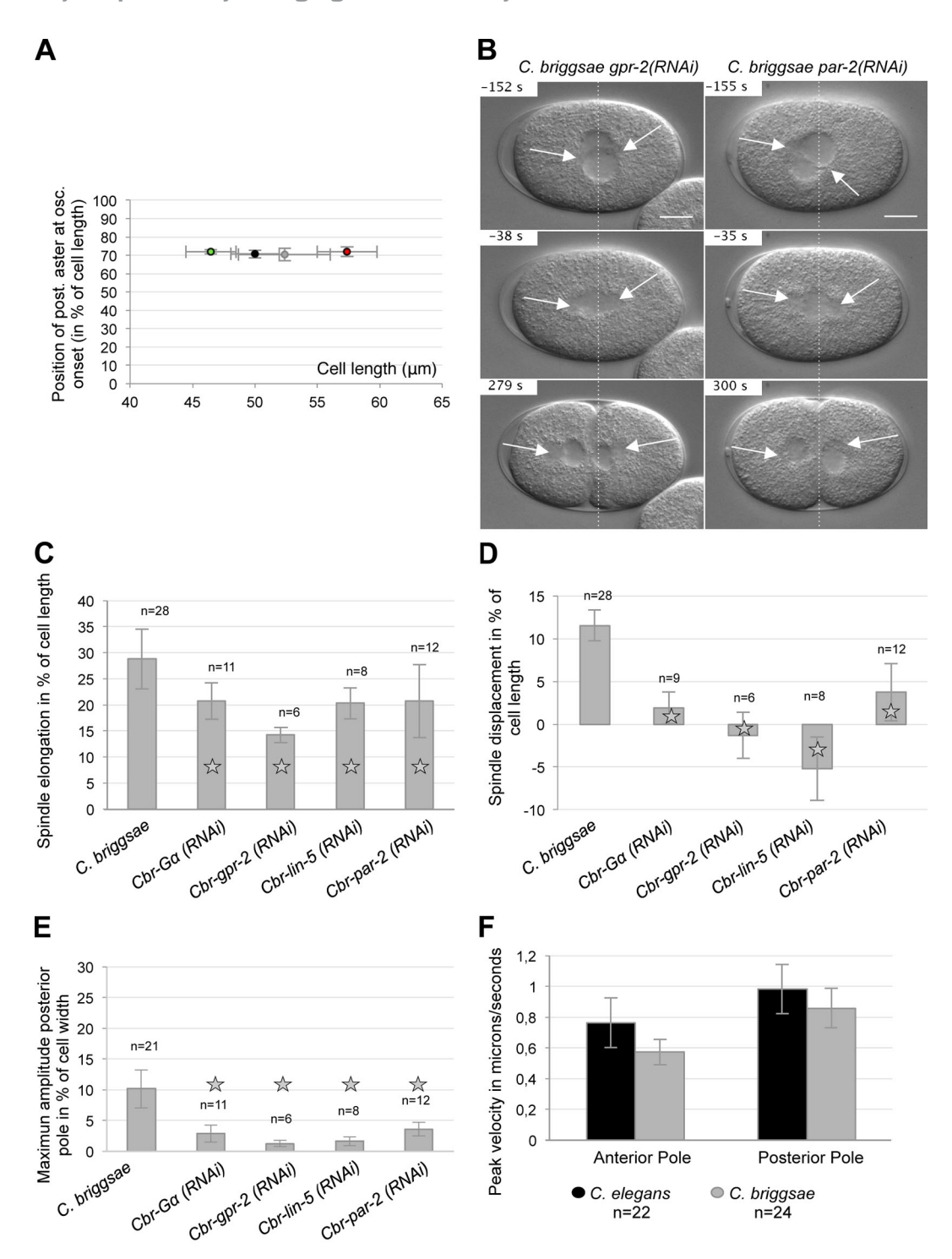


Figure S1. **G** α **-GPR-LIN-5-dependent unbalanced pulling forces control the first cell division of** *C. briggsae* **embryos.** (A) Position of the posterior centrosome (at oscillation onset) is shown relative to absolute embryo length in microns for wild-type *C. elegans* (n = 33) in black, wild-type *C. briggsae* (n = 28) in gray, short *C. elegans* embryos in green (after inactivation of the *cid-1* gene; n = 10), and long *C. elegans* embryos in red (after inactivation of the *C27D9.1* gene; n = 7). Regardless of embryo size, the centrosome starts to oscillate around 70% of embryo length. Error bars indicate standard deviation. (B) Snapshots from DIC recordings of *Cbr-gpr-2(RNAi)* and *Cbr-par-2(RNAi)* embryos. Time is shown relative to anaphase onset (t = 0 s). Anterior is to the left. Broken lines are positioned at 50% of embryo length. Arrows show the asters. Bars, 10 µm. (C–E) Measurements of spindle motion for n embryos of wild-type *C. briggsae*, *Cbr-Ga(RNAi)*, *Cbr-gpr-2(RNAi)*, *Cbr-lin-5(RNAi)*, and *Cbr-par-2(RNAi)*. Error bars indicate standard deviation. Statistical differences are shown with a star for comparison to wild-type *C. briggsae* (P < 0.05). (C) Initial spindle length (at metaphase onset) is subtracted from final spindle length (at cytokinesis onset), and is represented in percentage of cell length. (D) Initial position of the center of the spindle (at metaphase onset) is subtracted from position of the center of the spindle at cytokinesis onset. The distance is shown in percentage of cell length. Negative values correspond to an anterior shift of the spindle during anaphase. (E) Maximum amplitude of transverse oscillation of the posterior centrosome is measured in percentage of cell width. (F) The mitotic central spindle was severed using a laser microbeam at anaphase onset in both species. The mean peak velocity of released asters was measured in microns per second. Error bars indicate standard deviation.

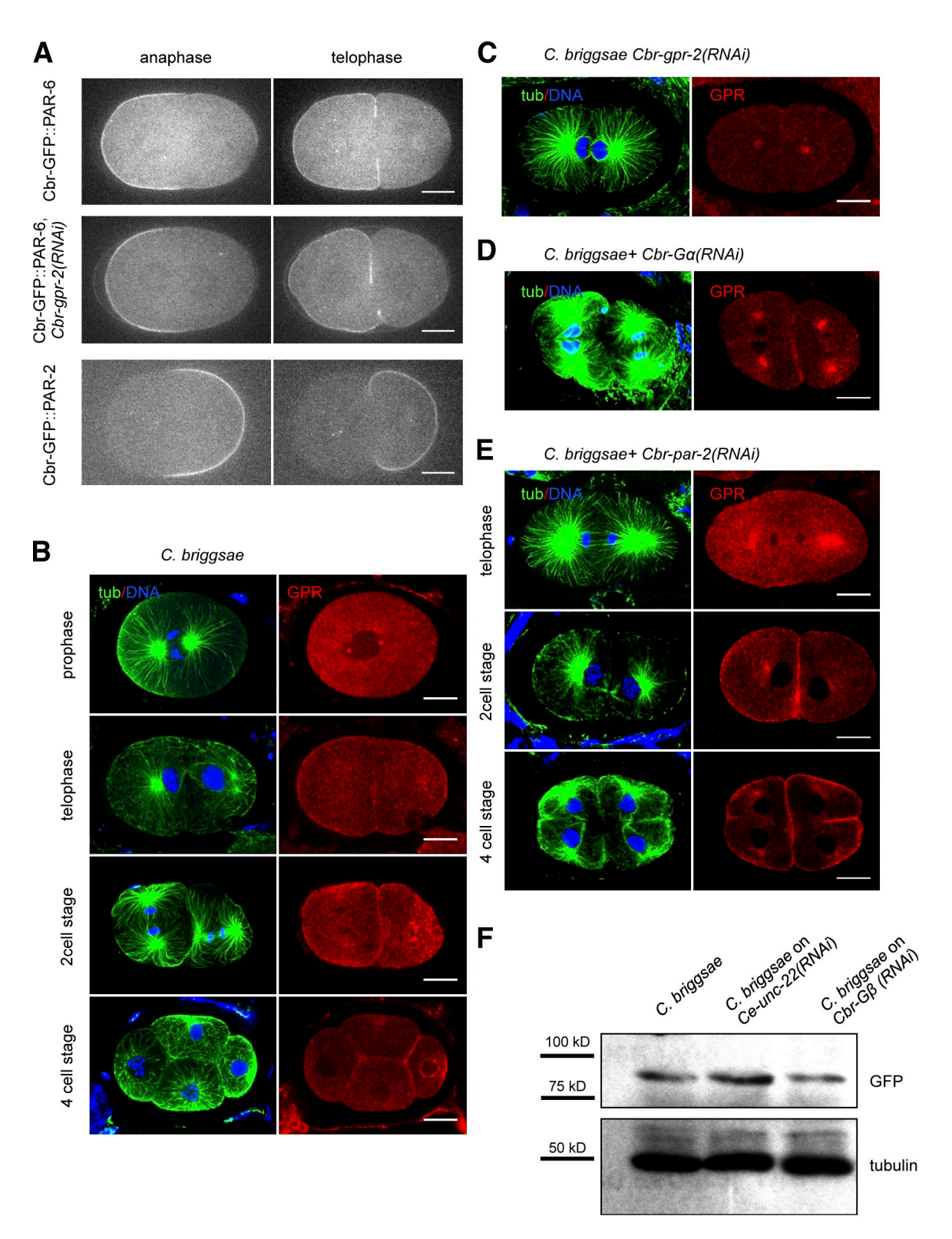


Figure S2. **Cbr-GPR-2 localization and levels in** *C. briggsae* **wild-type and RNAi-treated embryos.** (A) Snapshots of spinning disk movies from one representative embryo among 10 transgenic *C. briggsae* embryos expressing Cbr-PAR-6 or Cbr-PAR-2 fused to GFP. Anterior is to the left. As in *C. elegans*, PAR-6 and PAR-2 localize to opposite cortical domains. In the absence of *Cbr-gpr-2*, polarity is intact, confirming that, as in *C. elegans*, GPR-2 acts downstream of polarity proteins. (B–E) On all panels, microtubules are shown in green, DNA in blue, and GPR in red. The anterior pole is to the left. (B) *C. briggsae* wild-type embryos stained with an antibody against Cbr-GPR-2 at different stages. (C) *Cbr-gpr-2(RNAi)* telophase embryo stained with an antibody against Cbr-GPR-2 showing the specificity of the antibody for cortical and cytoplasmic signals. (D–F) Embryos expressing Cbr-GPR-2 fused to GFP were used, from transgenic lines showing no signs of GPR overexpression. (D) Embryos were subjected to *Cbr-par-2(RNAi)* and stained using an antibody against GFP. The cortical signal of GPR is strongly decreased. (E) Embryos were subjected to *Cbr-par-2(RNAi)* and stained using an antibody against GFP. GPR is found uniformly around the cortex and in the cytoplasm. (F) Embryos were treated with RNAi against *Cbr-Gβ* or the *C. elegans unc-22* gene as a negative control. Embryos were then prepared for protein extraction. The Western blot reveals GFP levels as a readout of GPR quantity in treated and untreated embryos. Tubulin was used as a loading control. Bars, 10 μm.



Video 1. **Time-lapse DIC recording of a wild-type** *C. elegans* **N2 embryo.** Images were acquired using a microscope (Axio Imager A2; Carl Zeiss) at 100×. Frames were captured every 0.5 s.



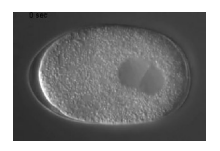
Video 2. **Time-lapse DIC recording of a wild-type** *C. briggsae* **JU1018 embryo.** Images were acquired using a microscope (Axio Imager A2; Carl Zeiss). Frames were captured every 0.5 s.



Video 3. Time-lapse DIC recording of a wild-type C. briggsae JU1018 embryo after laser severing of anterior astral microtubules using a pulsed N2 laser from a Leica LMD microscope (λ = 337 nm). Frames were captured every 0.5 s.



Video 4. Time-lapse DIC recording of a *C. briggsae* embryo treated with *Cbr-gpr-2(RNAi)*. Images were acquired using a microscope (Axio Imager A2; Carl Zeiss). Frames were captured every 0.5 s.



Video 5. Time-lapse DIC recording of a *C. briggsae* embryo from the ANA017 line, in which Cbr-GPR-2 is found in excess. Images were acquired using a microscope (Axio Imager A2; Carl Zeiss). Frames were captured every 0.5 s.



Video 6. **Time-lapse DIC recording of a** *C. briggsae* **embryo treated with** *Cbr-Gβ*(*RNAi*). Images were acquired using a microscope (Axio Imager A2; Carl Zeiss). Frames were captured every 0.5 s.



Video 7. **Time-lapse DIC recording of a** *C. briggsae* **embryo treated with** *Cbr-let-99(RNAi)*. Images were acquired using a microscope (Axio Imager A2; Carl Zeiss). Frames were captured every 0.5 s.

Table S1. Quantification of events associated with the first embryonic division in C. elegans and C. briggsae strains

			<u>-</u>				
Traits	C. elegans N2	C. elegans CB4856	C. elegans LKC34	C. briggsae JU1018	C. briggsae HK104	C. briggsae ED3092	C. briggsae JU1018 at 28°C
Embryo length (µm)	50.00 ± 1.95 (n = 33)	50.73 ± 2.01 (n = 23)°	50.92 ± 2.59 (n = 17)	52.37 ± 3.67 (n = 28)	52.56 ± 2.05 $(n = 25)^{b}$	51.00 ± 2.31 (n = 18)	ND
Embryo width (µm)	33.70 ± 1.46 $(n = 33)$	34.59 ± 1.47 $(n = 23)$	34.15 ± 1.50 $(n = 17)$	34.21 ± 1.92 $(n = 28)$	31.62 ± 1.70 $(n = 25)^{b}$	31.14 ± 1.46 $(n = 18)^{b}$	ND
Spindle length at metaphase onset (%)	26.48 ± 2.80 $(n = 19)^{\circ}$	ND	ND	24.48 ± 1.56 $(n = 16)^{b}$	ND	ND	ND
Spindle center at metaphase onset (%)	51.45 ± 1.66 $(n = 19)^{\circ}$	50.54 ± 3.56 $(n = 10)$	49.91 ± 0.87 $(n = 6)$	46.59 ± 1.56 $(n = 16)^{b}$	43.98 ± 2.31 $(n = 7)$	46.00 ± 2.69 $(n = 6)$	ND
Spindle length at anaphase onset (%)	29.72 ± 2.33 $(n = 19)$	ND	ND	28.30 ± 2.06 (n = 16)	ND	ND	ND
Spindle center at anaphase onset (%)	56.02 ± 1.83 $(n = 19)^{\circ}$	55.57 ± 3.72 (n = 12)	53.30 ± 1.07 $(n = 5)$	48.72 ± 1.59 $(n = 16)^{b}$	47.92 ± 1.20 (n = 8)	50.95 ± 2.37 $(n = 6)$	ND
Posterior aster position at anaphase onset (%)	70.85 ± 1.64 $(n = 33)^{\circ}$	70.09 ± 2.91 $(n = 23)^{\circ}$	69.84 ± 1.91 $(n = 15)^{\circ}$	62.89 ± 2.21 $(n = 28)^{b}$	62.65 ± 1.33 $(n = 17)^{b}$	66.90 ± 2.49 $(n = 18)^{b}$	ND
Posterior aster position at oscillation onset (%)	70.69 ± 2.14 $(n = 33)$	69.51 ± 3.30 (n = 23)	70.86 ± 2.46 (n = 16)	69.88 ± 3.00 $(n = 26)$	69.35 ± 2.60 $(n = 17)$	71.55 ± 3.32 (n = 18)	71.58 ± 2.92 (n = 8)
Time at oscillation onset (s)	-0.65 ± 8.58 $(n = 33)^{\circ}$	-4.59 ± 13.87 $(n = 23)^{\alpha}$	0.44 ± 15.55 $(n = 16)^{\circ}$	31.34 ± 12.47 $(n = 26)^{b}$	25.15 ± 11.55 $(n = 17)^{b}$	14.17 ± 14.62 $(n = 18)^{b}$	$(n = 8)^{b}$
Posterior aster at cytokinesis onset (%)	80.15 ± 1.34 $(n = 15)$	80.41 ± 2.30 $(n = 12)$	79.72 ± 1.06 $(n = 10)^{\circ}$	79.18 ± 1.83 $(n = 13)$	78.72 ± 0.97 $(n = 10)^{b}$	81.20 ± 1.56 $(n = 11)$	ND
Anterior aster at cytokinesis onset (%)	34.06 ± 1.46 $(n = 33)$	31.83 ± 2.11 $(n = 12)$	32.19 ± 1.32 $(n = 10)$	31.03 ± 1.19 $(n = 28)$	31.11 ± 1.49 $(n = 10)^{b}$	29.20 ± 1.62 $(n = 11)^{b}$	ND
Mean amplitude of posterior aster oscillation (%)	15.06 ± 3.61 $(n = 17)^{\circ}$	14.56 ± 2.56 $(n = 17)^{\circ}$	$(n = 9)^{\alpha}$	7.53 ± 2.37 $(n = 21)^{b}$	6.65 ± 2.00 $(n = 8)^{b}$	9.45 ± 2.65 $(n = 11)^{b}$	$(n = 6)^{b}$
Maximum amplitude of posterior oscillation (%)	18.99 ± 3.87 $(n = 17)^{\circ}$	18.60 ± 2.96 $(n = 17)^{\circ}$	$(n = 9)^{\alpha}$	10.14 ± 3.10 $(n = 21)^{b}$	9.20 ± 2.69 $(n = 8)^{b}$	$(n = 11)^{b}$	12.7 ± 4.95 $(n = 6)^{b}$
Mean frequency of posterior oscillation (mHz)	47.7 ± 12.4 (n = 17)	49.6 ± 9.2 $(n = 17)$	39.8 ± 4.0 $(n = 9)^{\alpha}$	46.3 ± 5.6 $(n = 21)$	45.9 ± 11.2 $(n = 8)$	52.3 ± 9.5 $(n = 11)$	62.4 ± 6.6 $(n = 6)^{b}$
Maximum amplitude of anterior oscillation (%)	11.21 ± 3.2 $(n = 33)^{\circ}$	ND	ND	5.36 ± 1.4 $(n = 25)^{b}$	ND	ND	ND
NEBD to cytokinesis (s)	282.6 ± 29.57 (n = 11)	ND	ND	277.2 ± 45.48 $(n = 9)$	ND	ND	ND

Three C. elegans and three C. briggsae wild-type strains recorded at 23°C are shown, as well as C. briggsae JU1018 animals raised and recorded at 28°C. Values represent means \pm SD. NEBD, nuclear envelope break down. n = the number of embryos per condition. Two-tailed Student's t test was used. °Statistical differences (P < 0.05) for comparison with C. briggsae JU1018. bStatistical differences (P < 0.05) for comparison with the C. elegans N2 strain.